Model and Fitting Results for the Filamentary Conduction in MIM Resistive Switching Devices

F. Palumbo[1], E. Miranda[2], G. Ghibaudo[3], and V. Jousseaume[4]

[1] CONICET-CNEA, Av. Gral Paz 1499, 1650, San Martin, Argentina.
[2] Departament d'Enginyeria Electrònica UAB, 08193, Bellaterra, Barcelona, Spain.
[3] IMEP-LAHC-MINATEC, 17 rue des Martyrs, 38054 Grenoble Cedex 9, France.
[4] CEA-LETI-MINATEC, 17 rue des Martyrs, 38054 Grenoble Cedex 9, France.

Experimental results for the resistive switching effect occurring in $Pt/HfO_2/Pt$ devices are analyzed within the framework of the two-terminal Landauer theory for mesoscopic conducting systems. It is shown that the magnitude of the current and the voltage dependence of the switching conduction characteristic are mainly dictated by the size of the filamentary path generated after electroforming. The temperature dependence of the high resistance conduction characteristics is also modeled in a consistent manner with the proposed picture.

Introduction

In the last decade, the interest in the resistive switching (RS) phenomenon in thin and thick dielectric films has impressively increased because of its implication for the nonvolatile memories industry (1,2). The so-called Resistive Random Access Memory, or succinctly RRAM, relies fundamentally on the reversible change of the resistance of a filamentary path generated across the oxide layer in a metal-insulator-metal (MIM) structure. The switching is often controlled by pulsed or ramped voltages. Remarkably, because of the extremely localized nature of the electron transport mechanism associated with RS, the active device area in a RRAM is very small, with lateral dimensions of only a few nanometers. This feature in combination with the possibility of interconnecting RRAMs using crossbar architectures (2) make these devices exceptionally relevant in terms of downscaling and potentially unbeatable in terms of fabrication costs.

The phenomenon has been reported for a wide variety of MIM structures with more or less similar characteristics and several studies have related RS to the rupture and recovery of conducting paths caused by the drift of atoms or vacancies and by Joule heating effects, respectively (1-4). In this regard, even though the origin of the switching behavior has received extensive consideration, the electron transport mechanisms corresponding to the high and low conduction states have not been investigated with such a great detail. Well-known transport models such as Poole-Frenkel, space charge limited conduction, or tunneling have been proposed to explain the conduction characteristics after electroforming but the fitting results are far from being conclusive. Alternatively, a number of models based on equivalent electrical circuits (5) are also available but in these cases the connection with the RS physics at microscopic level has not been completely developed.

In this work, we focus the attention on the current-voltage (I-V) characteristics associated with the low (LRS) and high (HRS) resistance states and in particular on the temperature dependence of HRS. These characteristics are analyzed within the framework of the two-terminal Landauer theory for mesoscopic systems (6,7). The central idea on which this theory is based is that the electrons flowing through a nanoscale constriction are subjected to lateral quantization effects. This constraint determines the transmission properties of the structure. Accordingly, the magnitude and functional dependence of the I-V characteristic is dictated by the local configuration of the conductive centers that form the filamentary path. In this context, a narrow or a wide constriction is related to HRS or LRS, respectively, in complete analogy with the soft and hard breakdown conduction modes in ultrathin oxides in MOS devices (8,9).

Sample Details and Resistive Switching Phenomenology

The devices used in this work are MIM structures with an area of $5x10^{-9}$ cm^2 and with a 10 nm-thick HfO_2 layer sandwiched in between Pt electrodes. The devices were fabricated at LETI in Grenoble, France (10). The characterization was carried out with a semiconductor parameter analyzer Keithley 4200 and using voltage sweep measurements (I-V) with current limitation (compliance).

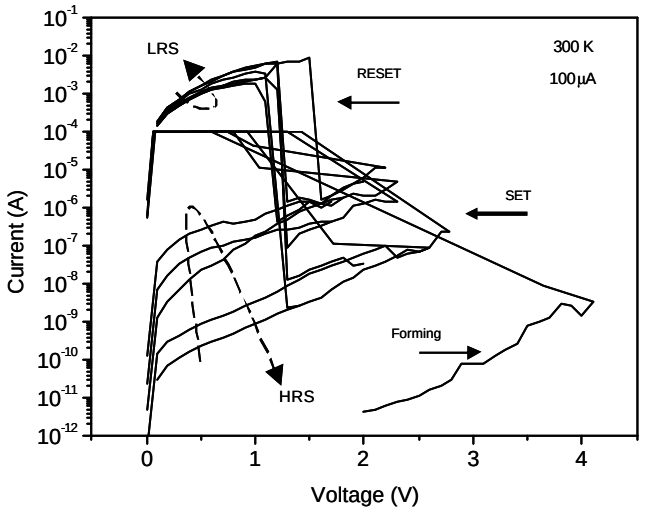

Figure 1. Typical electrical characteristics of MIM structures. Consecutives I-V curves showing transition between low resistive state (LRS) and high resistive state (HRS). A Forming/SET current compliance of 100µA is used at 300K.

Typically, an initial current-limited breakdown step is needed to generate the filamentary path. The forming process is characterized by a gradual increase of the current in low voltage range (likely tunneling), followed by a fast current runaway and a simultaneous voltage drop. In our case the forming voltage is around 4V. After this forming operation, the RS phenomenon is characterized by reversible transitions from HRS to LRS and viceversa following the application of a voltage ramp. The structure switches from

HRS to LRS after reaching a threshold voltage with current limitation (SET). The opposite transition from LRS to HRS (RESET) takes place at higher currents and lower voltages than the SET voltage. Figure 1 shows a typical RS behavior for consecutive I-V curves performed on the same device and with positive bias. The $Pt/HfO_2/Pt$ devices used in this study exhibit a switching behavior that does not depend on the polarity of the applied bias (unipolar switch).

Model for the Filamentary Conduction

The RS I-V characteristics shown in Fig.1 are modeled with the Landauer theory for mesoscopic conductors. The basic idea is that the electron transport is controlled by the local arrangement of the conducting centers that form the filamentary path. These centers are assumed to form a continuous confinement potential.

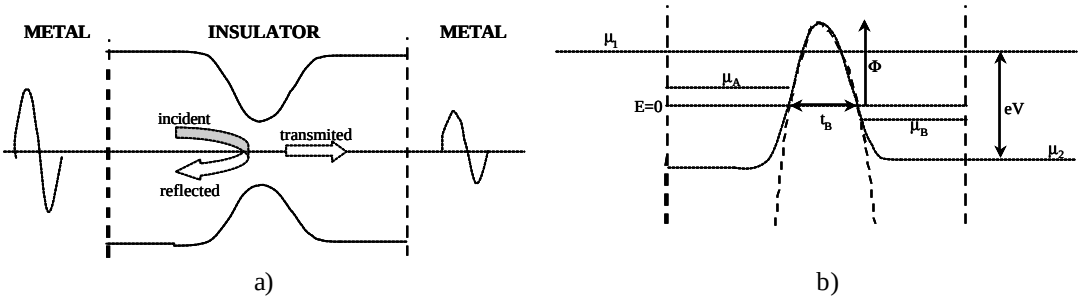

Figure 2. (a) Schematic diagram of the tube-like constriction associated with RS. (b) The barrier is a consequence of the tighter confinement effect. Φ is the barrier height and t_B the barrier width at the reference energy level ($E=0$).

Figure 2 shows a schematic diagram of the energy profile across the structure in the HRS case. The potential drops at the two ends of the conducting bridge arise as a consequence of the mismatch in the number of conducting modes at both sides of each connection and are associated with the contact resistance effect (6). The barrier is located at the constriction's bottleneck, which is supposed to be somewhere along the filamentary path. m_1 and m_2 are the quasi-Fermi levels deep inside the reservoirs so that $m_1-m_2=eV$ is the potential drop across the constriction, while m_A and m_B are the quasi-Fermi levels inside the constriction. $m_A-m_B \approx e(1-D)V$ is the potential drop across the tunneling barrier associated with the first quantized subband. D is the transmission probability. In the case of HRS, it could be assumed that the electrons trying to penetrate the barrier have energies $E<<\Phi$. According to the Landauer approach, the current that flows through a tube-like structure with a parabolic potential at its narrowest point (see Fig.2) reads (6,7):

$$I_{HRS} = \frac{4e}{ha}\frac{\exp[-a\Phi]}{\mathrm{sinc}(p\mathrm{k}\mathrm{T}a)}\sinh\left(\frac{aeV}{2}\right) \quad [1]$$

$$\text{with} \quad a = \frac{t_B p^2}{h}\sqrt{\frac{2m^*}{\Phi}} \qquad [2]$$

where Φ is the barrier height associated with the first quantized energy subband in the transversal direction, t_B its thickness at the reference energy level (E=0), T the absolute temperature, m^* the electron effective mass, e the electron charge, h the Planck's constant, and k the Boltzmann's constant. Notice that for T=0º K, this is the same equation used to model the soft breakdown I-V characteristic in ultrathin SiO_2 films in MOS structures (7).

On the other hand, for LRS, the constriction is wider and the electrons are assumed to have energies well above the top of the tunnelling barrier, so that D=1 for all the available transverse modes (N). In this case expression [1] can be simplified assuming a thinned potential barrier $t_B \to 0$. Therefore, from [2] $a \to 0$, so that expression [1] reads:

$$I_{LRS} = \frac{2e^2 N}{h} V = G_0 N V \qquad [3]$$

with $G_0 = 2e^2/h$ the quantum conductance unit. The linear relationship with the applied voltage [3] expresses that the filamentary path behaves as a ballistic conductor with N identical electron transport channels. However, it is worth pointing out that the hypothesis of N equal to a constant may be a bad approximation, since this number strongly depends on the specific form of the confining potential at the constriction's bottleneck. Moreover, notice that [3] is also independent of the temperature. Again this relies on the condition that the size of the constriction remains unaltered by increasing the temperature (N=constant).

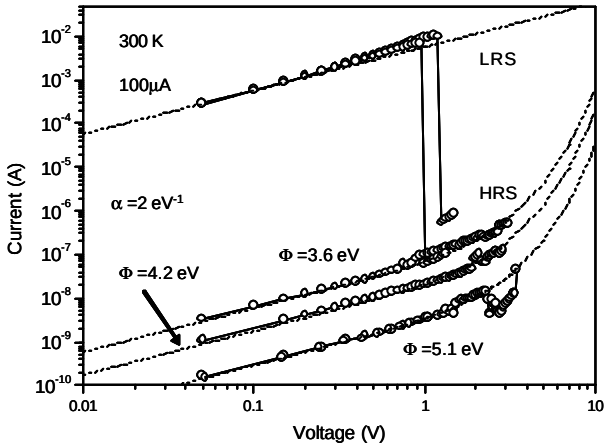

Figure 3. Typical RS I-V characteristics for the MIM structures investigated. Consecutives I-V curves showing transition between low resistive state (LRS) and high resistive state (HRS). A forming SET current compliance of 100 µA was used. The dashed lines correspond to fitting curves using expression (1) with α=2 eV^{-1}, and Φ ranging from 3.6 to 5.1 eV for the HRS, and N=70 in expression (3).

So far, we have shown that proposed approach accounts for the transition from HRS (exponential) to LRS (linear) in Fig.1 by varying the parameter a in eq.[1]. This result is a consequence of the vanishing (thinning) of the potential barrier as t_B or a tends to zero. Figure 3 shows some fitting results to typical LRS and HRS I-V curves using eqs. [1] and [3]. The agreement is very good, especially for the HRS case (a=2 eV^{-1} and Φ values ranging from 3.6 to 5.1 eV). From eq.[2], these parameter values correspond to barrier thicknesses in the range from 1.4 nm to 1.7 nm for an effective mass m^*=0.11m (11), with m the free electron mass. The spread of the experimental curves is typical of a current-limited dielectric breakdown phenomenon such as soft breakdown. In the case of the LRS I-V curves, large values of N (~70) had to be considered in order to achieve acceptable fitting results. As mentioned, this puts a serious warning on the assumption of a constant density of transverse energy levels as considered in eq.[3].

Temperature Dependence of Resistive Switching

In this Section, we focus the attention on the temperature dependence of the RS mechanism. Figure 4(a) shows some typical I-V characteristics with transitions from LRS to HRS measured on different devices and with temperatures ranging from 77 K to 300 K. Notice that the HRS and LRS curves exhibit similar slopes (~1) at very low voltages, which is consistent with the proposed model. Figure 4(b) illustrates the details of such agreement. For clarity only two HRS I-V curves are shown (300 K and 90 K). The parameters for the model curves are a=2 eV^{-1}, Φ =1.35 eV for 300 K and a=2.8 eV^{-1}, Φ =4.2 eV for 90K.

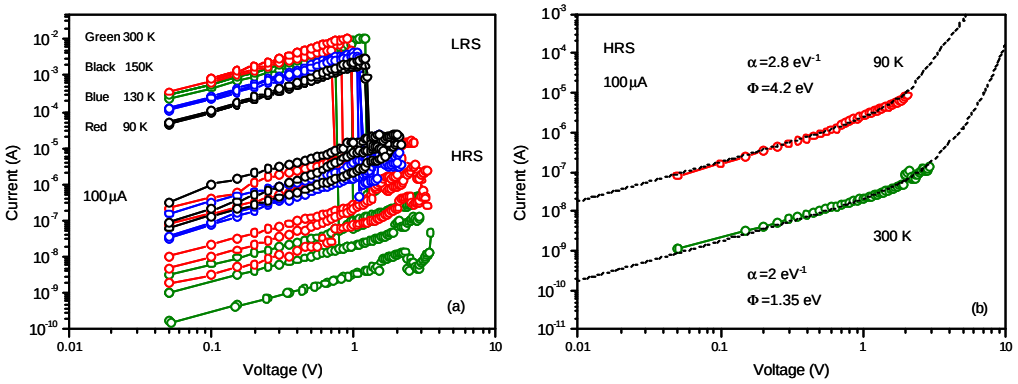

Figure 4. (a): Consecutives I-V curves showing transition between low resistive state (LRS) and high resistive state (HRS) for different samples at different temperatures. A Forming/SET current compliance of 100μA was used. Green, black, blue and red correspond to 300, 150, 130 and 90 K respectively.
(b) Current voltage characteristics for the high resistive state (HRS) at different temperatures. Green and red curves correspond to 300, and 90 K respectively. The dashed lines correspond to fitting curves of expression [1] using α=2 eV, and Φ_B =1.35 eV for 300K and α=2.8 eV, and Φ_B =4.2 eV for 90K.

Figure 5 shows the model parameters for the theoretical HRS curves (t_B and Φ in eq.(2)) as a function of temperature. The thickness of the barrier t_B is calculated from the fitting parameters (α and Φ) using eq.[2]. It is clear that the parameters do not vary systematically for the entire range of T giving indication that the I-V curves for the HRS maintain the same characteristics for different temperatures as reported in Fig. 4(a). As a general observation, it is not possible to establish clear temperature dependence for the localized current in our samples. However, it is worth pointing out that the parameters shown in Fig.5 are within a physically reasonable range for what is expected for a nanoscale filamentary conducting path.

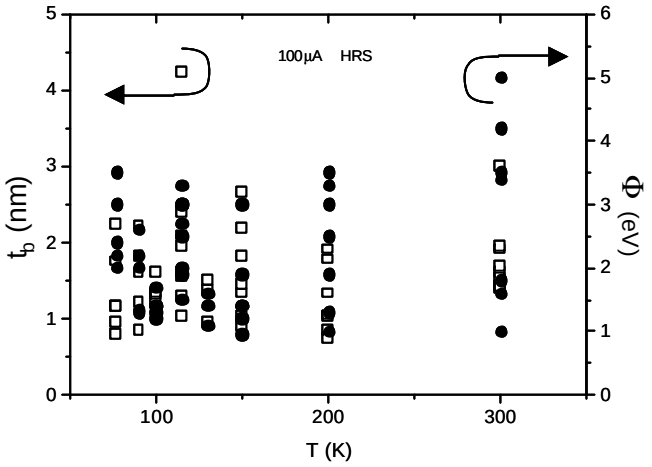

Figure 5. Parameters of the theoretical curves for HRS, t_B and Φ of eq.[2], as function of temperature ranging from 77K to 300K.

Summary

Experimental results for the resistive switching mechanism in Pt/HfO_2/Pt structures were analyzed using the Landauer formula for electron transport in mesoscopic devices. The difference between the high and low resistance states was ascribed to the size of the constriction that bridges the two electrodes. It was shown that the limiting forms of the general transport model leads to current equations compatible with the observed conduction modes in a wide range of temperature (77K-300K).

Acknowledgments

This work has been partially supported by PIP-1063 CONICET and PICT07-01143 ANPCyT, Argentina. E.M. acknowledges the economical support from the International Centre of Theoretical Physics (ICTP), Trieste, Italy under the Visitor Scientist Program, the funding of the Spanish Ministry of Science and Innovation under contracts ACI2009-0853, TEC2009-09350, and the DURSI of the Generalitat de Catalunya under contract 2009SGR783.

References

1. R. Waser, R. Dittmann, G. Staikov, K. Szot, Adv. Materials 21, 2632-2663 (2009)
2. A. Sawa, Materials Today 11, 28-36 (2008)
3. D. Kim, S. Seo, S. Ahn, D. Suh, M. Lee, B. Park, I. Yoo, I. Baek, H. Kim, E. Yim, J. Lee, S. Park, H. Kim, U. Chung, J. Moon, B. Ryu, Appl. Phys. Lett. 88, 202102 (2006)
4. M. Sánchez, M. Rozenberg, I. Inoue, Appl. Phys. Lett. 91, 252101, (2007)
5. K. Szot, W. Speier, G. Bihlmayer, and R. Waser, Nature Materials, 5, 312-320, (2006).
6. S. Datta, *Electronic Transport in Mesoscopic Systems*, Cambridge Press (1997).
7. E. Miranda, C. Walczyk, C. Wenger and T. Schroeder, IEEE Elect. Dev. Lett. Vol. 31, No 6, 609 – 611, (2010).
8. E. Miranda, J. Suñé, Proceedings 39th IEEE International Reliability Physics Symposium, 367-379, (2001).
9. E. Miranda, J. Suñé, Microelectron. Reliab. 44,1, (2004)
10. V.Jousseaume, A. Fantini, J. Nodin, C. Guedj, A. Persico, J. Buckley, S. Tirano, P. Lorenzi, R. Vignon, H. Feldis, S. Minoret, H. Grampeix, A. Roule, S. Favier, E. Martinez, P. Calka, N. Rochat, G. Auvert, J. Barnes,P. Gonon, C. Vallée, L. Perniola, and B. De Salvo, Proceedings 19th IEEE International Memory Workshop (2010).
11. S. Monaghan, P. Hurley, K. Cherkaoui, M. Negara, and A. Schenk, Solid State Electron. Vol.53 No.4 pp. 438-444, (2009).